High-visibility interferometric measurement of the diffraction phase

Salvador Barraza-Lopez

Department of Physics and Beckman Institute for Advanced Science and Technology, University of Illinois at Urbana-Champaign, Urbana, Illinois 61801, USA, and Department of Physics, Virginia Tech, Blacksburg, Virginia 24061, USA

Daniel F. V. James

Department of Physics and Institute of Optical Sciences, University of Toronto, 60 St. George Street, Toronto, Ontario, M5S 1A7 Canada

Paul G. Kwiat

Department of Physics, University of Illinois at Urbana-Champaign, Urbana, Illinois 61801, USA

Received July 3, 2006; revised November 24, 2006; accepted November 29, 2006; posted December 8, 2006 (Doc. ID 72565); published March 14, 2007

We obtain the absolute phase in Fresnel diffraction for Gaussian beams by using a modified polarization Sagnac interferometer in which counterpropagating paths are spatially separated and labeled according to polarization. By erasing the polarization "which-path" information with an analyzing polarizer situated after the modified interferometer, we are able to regain interference and to precisely control the relative intensities of the diffracted and the reference beams. The resulting optimized visibility allows for a precise phase determination. This setup is very stable, requiring no active elements. © 2007 Optical Society of America

OCIS codes: 050.1940, 120.5050, 120.3180, 120.2650.

1. INTRODUCTION

The diffraction of light is critical in many optical data storage applications, so a deep understanding of it is essential for their design and optimization.[1] For example, the rapid divergence of the beam as it emerges from the front facet of a diode laser is due to diffraction; diffraction from edges on the grooves of an optical disc surface is used to generate tracking-error signals; and some schemes for readout of recorded data also utilize diffraction from edges of pits and magnetic domains. Many of these applications employ focused Gaussian beams. Diffraction effects also play an important role in other experimental systems, such as neutron-scattering experiments[2] and atom optics[3] (where the high gradient produced by a diffracted optical beam may be used to create an atom or molecule mirror).

Despite the long history of attention to the *intensity* in diffraction, relatively little has been paid to the *phase*, which requires interfering the diffracted beam with a reference electromagnetic field. For example, a beam may be split in an interferometer, and a straight edge introduced into one of the paths. The interference profile after recombination of the beams contains information regarding the phase of the diffracted field. However, a problem arises, since the amplitude of the diffracted beam decreases rapidly in the so-called shadow region: even though interference effects are present in the recombined beam, the low visibility due to the difference in intensities of the two interfering fields makes extracting the Fresnel phase burdensome. In previous work this required an active (electromechanical) dithering element and an additional attenuation of the reference beam.[4]

In this paper we present a different approach, inspired by *quantum erasure* experiments, although our experiment has a completely classical explanation; only with nonclassical input states (e.g., single-photon Fock states) would it require a quantum description. From Ref. [5], the basic elements of a quantum eraser are the interfering quantum systems, a method of introducing which-path information, and a method of subsequently erasing this information in order to restore interference. In the present case our interfering system is a laser beam, the which-path information corresponds to polarization labels on the interfering paths, and the erasure and accompanying tuning of the visibility are performed by an analyzing polarizer placed after the interferometer. We employ a somewhat novel displaced polarization Sagnac interferometer, which affords us much greater stability. We have used this to obtain the phase information in Fresnel diffraction by a straight edge for Gaussian beams.

In Section 2 we provide a description of the plane-wave scalar theory of near-field diffraction in terms of Cornu's spiral. Section 3 is devoted to the technique for extracting the Fresnel phase, with particulars of our experimental setup described in Section 4. Our results for unfocused and focused beams are included in Section 5, and conclu-

sions are presented in Section 6. Appendix A contains mathematical details concerning the description of propagating Gaussian beams.

2. FRESNEL DIFFRACTION FOR GAUSSIAN BEAMS

The investigation of diffraction of a Gaussian beam by a straight edge has been treated by a number of authors. Pearson *et al.*[6] were among the first to provide a theoretical and experimental study. The theoretical description is based on the Kirchhoff–Fresnel scalar theory[7] as applied to a TEM_{00q} laser mode. The intensity diffraction patterns were calculated for different sizes of the beam waist, with experimental measurements predominantly near intensity maxima and minima. Their finding that, for extreme focusing, the fringes wash out was explained by Sambasivan.[8] Later, an alternative approach for the numerical calculation of diffraction intensities in terms of Gaussian modes was provided, in which beam intensity is expressed in terms of Hermite- or Laguerre-basis functions, and the coefficients on the beam's amplitude are obtained recursively.[9] However, in this case the quality of the diffraction pattern for a straight edge is poor even with as many as 500 basis functions, as additional oscillations in the diffraction pattern are still observable. A full 3-D vector calculation of electromagnetic straight-edge diffraction was reported recently (Ref. [10] and references therein), though this is beyond what we require here.

For completeness we give here a brief synopsis of the analysis of the straight-edge diffraction problem. Figure 1 shows schematically the system under consideration. A Gaussian beam is incident from the left along the z axis (defined to be the axis of symmetry of the beam) onto a straight edge placed along the y direction at a distance x_1 from the center of the beam and blocking the incoming field for $x<x_1$. The plane of maximum intensity defines $z=0$, the location of the beam waist. The distance from the waist to the straight edge is z_1. The field $\mathcal{U}_0$ associated with a Gaussian beam at the point (x',y',z') is given by[11]

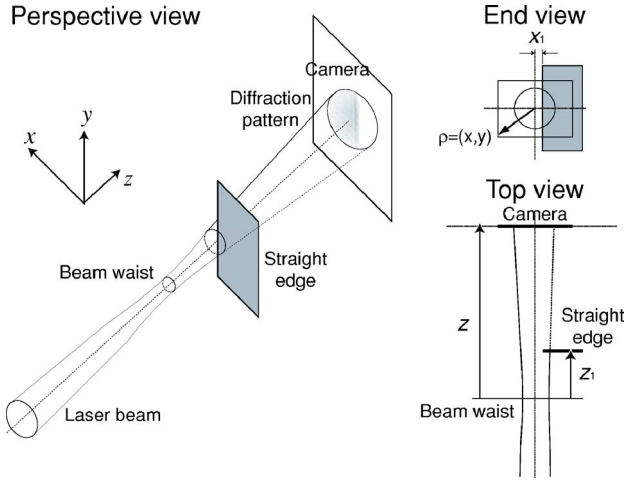

Fig. 1. Geometry of diffraction of a Gaussian beam by a straight edge.

$$\mathcal{U}_0(\boldsymbol{\rho}',z') = -i\frac{AZ_0}{q(z')}\exp(ikz')\exp\left[\frac{ik}{2q(z')}\boldsymbol{\rho}'^2\right]. \quad (1)$$

Here, $k\equiv 2\pi/\lambda$ is the wavenumber, $\boldsymbol{\rho}'=(x',y')$ is the transverse radial vector, A is the amplitude of the field at the origin, $q(z')\equiv z'-iZ_0$, and Z_0 is the Rayleigh range of the beam. The Rayleigh range characterizes the distance that a Gaussian beam can propagate before significant spreading occurs and depends on the radius W_0 of the laser beam waist: $Z_0\equiv kW_0^2/2$. According to Fig. 1 the field incident at the plane of the straight edge is given by $\mathcal{U}_0(\boldsymbol{\rho}',z_1)$. The diffracted field $U_d(\boldsymbol{\rho},z)$ at some point (x,y,z) beyond the straight edge arises from the contributions of the wavefronts not interrupted by the straight edge (those for which $x>x_1$), given in terms of the Huygens–Fresnel principle and approximated by the Fresnel diffraction formula[12]:

$$U_d(\boldsymbol{\rho},z) = -\frac{ik\exp[ik(z-z_1)]}{2\pi(z-z_1)}\int_{-\infty}^{+\infty}dy'\int_{x_1}^{+\infty}dx'\mathcal{U}_0(x',y',z_1)\times\exp\left[i\frac{k(\boldsymbol{\rho}-\boldsymbol{\rho}')^2}{2(z-z_1)}\right], \quad (2)$$

where $\boldsymbol{\rho}=(x,y)$. After algebraic manipulation and evaluation of the integral over the y' direction (see Appendix A), Eq. (2) reduces with no further approximations to

$$U_d(\boldsymbol{\rho},z) = \frac{\mathcal{U}_0(\boldsymbol{\rho},z)}{2}[1+(i-1)(C(w)+iS(w))] \equiv |U_d(\boldsymbol{\rho},z)|\exp[i\phi(w)], \quad (3)$$

where $\mathcal{U}_0(\boldsymbol{\rho},Z)$ is the amplitude of the undiffracted beam at the screen (i.e., the amplitude that would be observed *without* the straight edge present) and $\phi(w)$ is the Fresnel phase. $C(w)$ and $S(w)$ are the well-known Fresnel integrals

$$C(w)\equiv\int_0^w dt\cos\left(\frac{\pi t^2}{2}\right), \qquad S(w)\equiv\int_0^w dt\sin\left(\frac{\pi t^2}{2}\right), \quad (4)$$

where $w=w(x,z)$ is the *scaled length* in the observation plane (for a plane orthogonal to the direction of propagation, as in the present case, z remains fixed), a complex number given by (see Appendix A)

$$w(x,z) = \sqrt{\frac{k(z-iZ_0)}{\pi(z_1-iZ_0)(z-z_1)}}\left(x_1-\frac{z_1-iZ_0}{z-iZ_0}x\right). \quad (5)$$

The argument w is, in general, required to be complex (with an implied analytical continuation of the Fresnel integrals) to describe the diffraction of *Gaussian* beams. However, for well-collimated beams the Rayleigh range Z_0 is large ($Z_0/z_1\gg 1$); hence, two simplifying approximations can be made. First, we need consider only the first term (a real number) in the asymptotic expansion of Eq. (5):

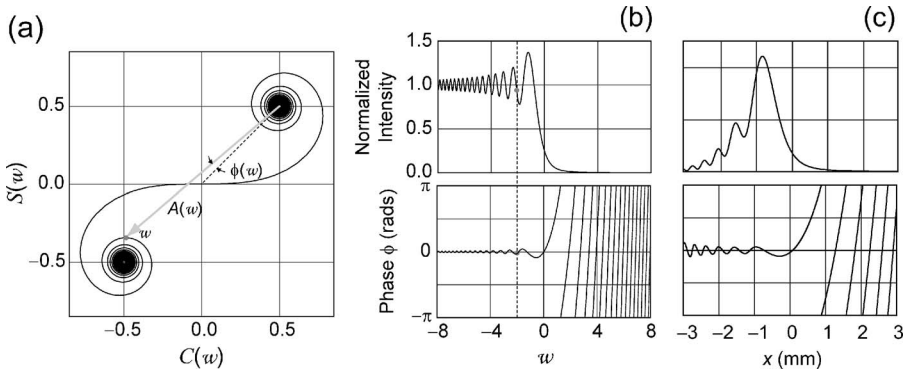

Fig. 2. (a) Cornu's spiral and (b) intensity and phase profiles for the case of a straight edge blocking the semi-infinite plane (x,y) for $x\leq 0$ $(w\geq 0)$, assuming an incident plane wave. (c) Typical intensity and phase profiles for a tightly focused Gaussian beam.

$$\lim_{z_0/z_1\to\infty} w = \sqrt{\frac{k}{\pi(z-z_1)}}(x_1-x). \tag{6}$$

Also, we can approximate $\mathcal{U}_0(\boldsymbol{\rho},z)$, which has the beam profile information, by a simple Gaussian envelope $\exp[-\beta\rho^2]$ with β a real, positive fitting parameter. This way $\mathcal{U}_0(\boldsymbol{\rho},z)$ adds, at most, a constant phase to the diffraction pattern. These approximations were also employed in Ref. [2] and are suitable for our first set of measurements, where we used a well-collimated beam. Furthermore, we assume $x_1=0$, so that the straight edge passes through the center of symmetry of the beam profile. As z remains fixed once an observation plane perpendicular to the direction of propagation is chosen, a variation of w becomes linearly dependent on x only. A well-known graphical representation in the complex plane of the normalized diffraction $[\mathcal{U}_0(\boldsymbol{\rho},z)=1]$ for real w, i.e., incident plane waves, is known as Cornu's spiral[7] and is shown in Fig. 2(a). Here the Fresnel integrals are represented for all real values of w. For an obstacle blocking the incoming field for $x\leq 0$, the *intensity* $I(w)$ [Fig. 2(b), top] of the beam for an arbitrary w is calculated as half the *squared* magnitude of the vector [shown in gray in Fig. 2(a)] joining the point (1/2,1/2)—corresponding to $(\lim_{w\to\infty} C(w), \lim_{w\to\infty} S(w))$—with the point parameterized by $w:(C(w),S(w))$. In a similar way, for plane waves the phase ϕ [Fig. 2(b), bottom] is a function of w only and is given by the argument of Eq. (3), $\phi(w)=\arg(U_d(w)) - \phi_{-\infty}$, where $\phi_{-\infty}$ is obtained by requiring the phase $\phi(w)$ to be zero far enough from the straight edge: $\lim_{w\to-\infty}\phi(w)=0$.

Our motivation for including these standard facts is to emphasize that while the intensity of the field goes to zero for $w>0$ (the shadow region), from Cornu's spiral we can easily see that it is precisely for these values of w that the strongest phase oscillations occur. This fact will not be strongly modified for a focused Gaussian beam, though the particular details of the intensity and phase oscillations are different, as shown by plotting the intensity and phase from Eq. (3) in Fig. 2(c).

3. DETERMINATION OF THE FRESNEL PHASE

As mentioned in Section 1, our method uses orthogonally polarized beams: a beam originally polarized at 45° is split in an interferometer into two beams of equal intensity with horizontal $(H)\equiv\begin{pmatrix}1\\0\end{pmatrix}$ and vertical $(V)\equiv\begin{pmatrix}0\\1\end{pmatrix}$ polarization (see Fig. 4). With the straight edge in the V-polarized path, the total field after the beams are recombined is the coherent superposition of fields with amplitudes $\begin{pmatrix}|\mathcal{U}_0|/\sqrt{2}\\0\end{pmatrix}$ and $\begin{pmatrix}0\\|U_d(w)|/\sqrt{2}\end{pmatrix}e^{i(\phi(w)+\delta)}$, where we have omitted the dependence of $\mathcal{U}_0$ and U_d on $\boldsymbol{\rho}$ and z, but we have included the possibility of an extra dynamical phase shift δ due to a path-length imbalance. No interference is observed because the polarizations are orthogonal, i.e., because the underlying processes are not, in principle, indistinguishable. By using an analyzing polarizer, one can "erase" the distinguishing polarizations and recover interference.[5] Moreover, when the polarizer is appropriately oriented at an angle θ (defined with respect to H polarization), the relative intensities of the beams can be precisely tuned:

$$\begin{aligned} I(\theta,w) &= \frac{1}{2}\left|\begin{pmatrix}\cos\theta, & \sin\theta\end{pmatrix}\begin{pmatrix}|\mathcal{U}_0|\\|U_d|e^{i(\phi(w)+\delta)}\end{pmatrix}\right|^2 \\ &= \frac{1}{2}(|\mathcal{U}_0|^2\cos^2\theta + |U_d(w)|^2\sin^2\theta \\ &\quad + |\mathcal{U}_0||U_d(w)|\sin(2\theta)\cos[\phi(w)+\delta]). \end{aligned} \tag{7}$$

By equalizing the relative intensities of the reference and diffracted beams, we can greatly improve the contrast between consecutive minima and maxima in the interference profile, even when the intensity from the diffracted beam is greatly reduced, i.e., in the shadow region. Specifically, on the basis of Eq. (7), for any value of w (and hence for any value of x on the observation plane), there exists an analysis angle θ such that the fringe visibility in the vicinity of $w(x)$ reaches 100%; this occurs when θ satisfies $-|\mathcal{U}_0||U_d(w)|\sin(2\theta)=|\mathcal{U}_0|^2\cos^2\theta+|U_d(w)|^2\sin^2\theta$.

To better appreciate the usefulness of this technique, we compare the intensity predicted by Eq. (7) with the intensity after a standard Mach–Zehnder interferometer using unpolarized beams:

$$I(w) = \tfrac{1}{2}(|\mathcal{U}_0|^2 + |U_d(w)|^2 + 2|\mathcal{U}_0||U_d(w)|\cos[\theta(w)+\delta]). \tag{8}$$

As $U_d\to 0$ in the limit $w\gg 0$, poor visibility is obtained in the shadow region unless additional attenuation is in

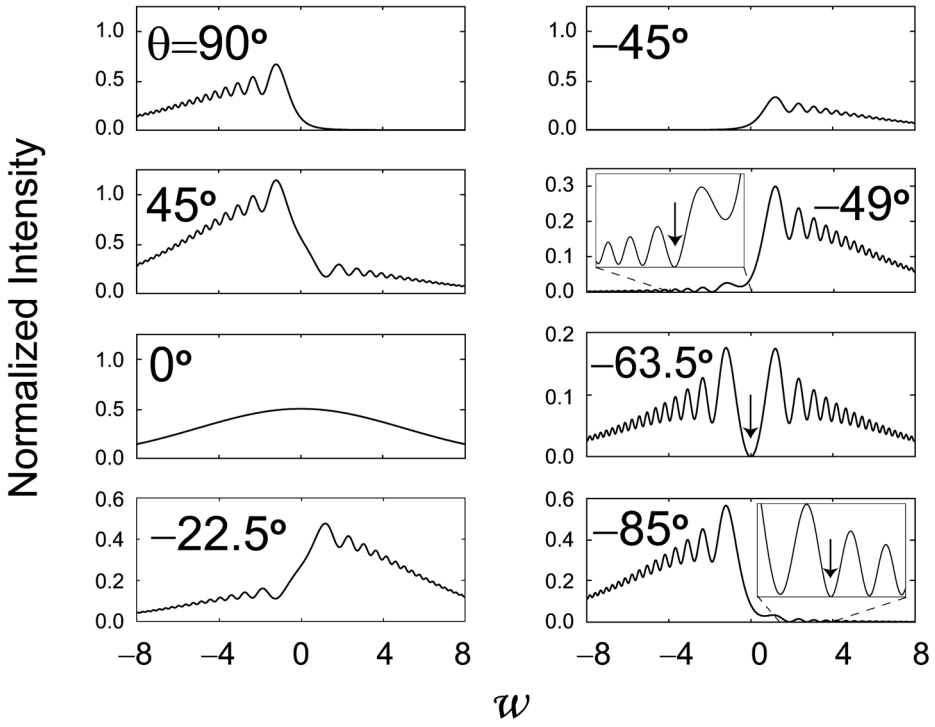

Fig. 3. Intensity profiles from Eq. (7) for selected analyzer angles. For $\theta=90°$ (the diffracted, V-polarized beam) the familiar straight-edge diffraction pattern appears. $\theta=0°$ gives the intensity from the H-polarized reference beam. The plot at 45° shows the combined intensity when the analyzing polarizer has the same polarization as the beam entering the interferometer. The plot at −45° shows an apparent inversion of the diffracted beam with respect to $w=0$, although its intensity is smaller. The other analysis angles show the tuning of the minima at different values of w (positive, zero, and negative, see vertical arrows) for θ in the (−90°, −45°) interval, implying a perfect visibility with respect to the neighboring intensity maxima. The maximum achievable visibility decreases outside the (−90°, −45°) interval, as stressed in the −22.5° subplot.

place, making phase determination difficult in the presence of noise. In our approach, we can apply this attenuation *outside* the interferometer, so that it does not affect the value of δ. In the previous work by Boyd and Moore,[4] the determination of the Fresnel phase required varying δ with a piezoelectrically driven oscillating mirror. As discussed below, our use of a Sagnac configuration (for which $\delta=0$) obviates the need of active, oscillating components, thus making the interferometer extremely stable.

In Fig. 3 we have plotted a number of normalized intensity profiles based on Eq. (7) for different analysis angles. At $\theta=0°$, only the reference beam is seen. At 90°, only the contribution due to the diffracted beam is seen. For other angles the effect of the Fresnel phase starts to be visible for $w>0$. At −45° the resulting profile appears as an (attenuated) reflection of the original Fresnel intensity profile; this occurs solely because of this particular analysis angle and no other manipulation of the beams. For selected θ's in the open interval (−90°, −45°), one can bring a given local minimum to be strictly zero, as emphasized by the vertical arrows in the subplots at −49°, −63.5° and −85°.

4. EXPERIMENTAL SETUP

Our experimental setup is shown in Fig. 4. A beam from a ~1 mW He–Ne laser ($\lambda=633$ nm) is directed through a single-mode optical fiber (which prepares a clean input mode, in addition to attenuating the beam) and collimated to a ~4 mm wide beam. The beam then traverses a

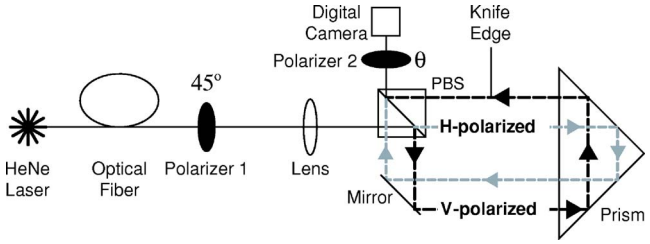

Fig. 4. Schematic view of our experimental setup. A coherent beam from a He–Ne laser is split in a modified Sagnac interferometer into two paths labeled with orthogonal polarizations. We place a knife edge into the outermost path and tune the relative intensities from each contributing path, using a polarizer at θ, prior to recording the resulting image. PBS stands for polarizing beam splitter.

polarizer at 45° before entering a modified Sagnac interferometer. A Sagnac configuration is ideal for our application because it is intrinsically stable and does not add additional relative phases to the counter circulating beams, i.e., $\delta=0$. Our modifications to the usual Sagnac can be summarized as follows.

1. We replace the unpolarized 50/50 beam splitter with a *polarizing* beam splitter (PBS). Polarization Sagnac interferometers have been previously employed[13,14] for high-precision measurements (including gyroscopes and potentially gravitational wave detectors,[15,16] surface profiling of mirrors,[17] and high-sensitivity magneto-optical measurements[18]) and in novel sources of polarization-entangled photons.[19] In our case, the beams counter-

propagating in the interferometer become labeled: clockwise → horizontal polarization; counterclockwise → vertical polarization. Because the incoming beam was polarized at 45°, the intensities of the counterpropagating beams are nominally identical, each with a power of ~200 nW.

2. We displace the bottom-left mirror of the Sagnac outward (see Fig. 4), spatially separating the two beams. (Displaced, unpolarized Sagnac interferometers have been used to optically implement Grover's search algorithm.[20]) While such displacement does *not* modify the relative path lengths of the beams inside the interferometer, and thus adds no additional phase, it enables us to partially block one of the propagation directions without blocking the other.

3. We place a knife edge (a blackened razor blade) in the most accessible outer path of the interferometer, so that the knife edge blocks the field for $x<0$ (cf. Fig. 1). The distance $(z-z_1)$ from knife edge to the screen of the digital camera (Fig. 1) is 35 cm. The intensity and phase expected for this path are those shown in Fig. 2(b), except for a slowly varying Gaussian envelope function multiplying the intensity profile.

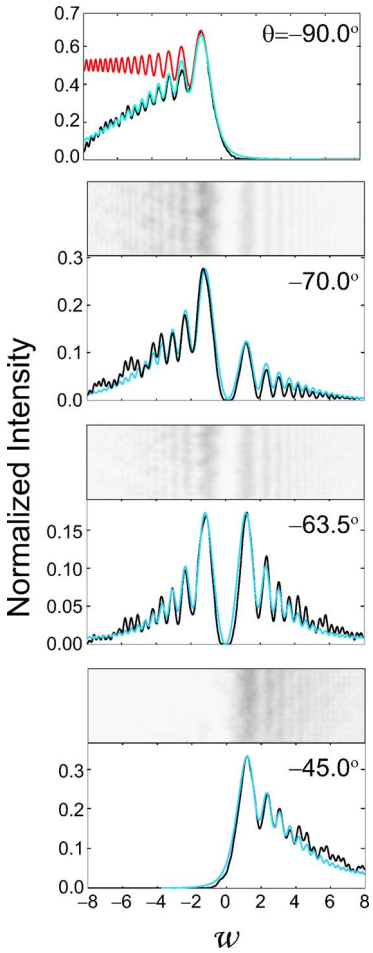

Fig. 5. (Color online) Intensity profiles for four analyzer settings. Black curves correspond to the measured data. Light gray (blue online) in all panels curves are theoretical predictions employing Cornu's spiral and a best-fit Gaussian envelope. The knife edge blocks the right half of the beam. $\theta=\pm 90°$ corresponds to vertically polarized light (path with knife edge), and $\theta=0°$ corresponds to horizontally polarized light (path with no obstacle). For $\theta=-90°$ we also display the theoretical normalized intensity [upper (red online) curve in top panel] with no envelope function.

Before photographing the beams with a CCD digital camera (Cohu High Performance Monochrome Interline Transfer CCD Camera 4900 Series, with a 6.4 mm wide collecting array), we direct them through a second polarizer at angle θ, allowing measurement of the combined beams with tunable contributions from orthogonal polarizations. As described above, this can improve the fringe visibility at a given position and, therefore, the accuracy in determining the Fresnel phase.

5. INTENSITY PROFILES FOR GAUSSIAN BEAMS

A. Fresnel Phase for Collimated Beams

In our first set of measurements we employed an approximately collimated beam with a $1/e^2$ diameter of $2W_0=2.0$ mm. To obtain intensity profiles from the camera image, we used data acquisition software to select a rectangular section of the picture (6 mm wide by 1.5 mm high) centered on the image. The resulting intensity profile was then averaged over the vertical direction of the snapshot. Four such averaged intensity profiles are shown in Fig. 5, with accompanying photographs in three instances. At $\theta=-90°$, only light from the path containing the knife edge is seen. The intensity as obtained from theory is shown in red and in blue (online) when multiplied by the best-fit Gaussian envelope. The black curve corresponds to the experimental data. The subsequent plots show intensities for $\theta=-70°$, $-63.5°$, and $-45°$; the same Gaussian envelope is used for all theoretical curves. We see quite good agreement, particularly in the locations of the minimum and maximum intensities. Discrepancies between theory and experiment are mainly due to slight spatial nonuniformities in the incident beam (cf. structures in plots 1, 2, and 5 in Fig. 6), probably due to dust particles, nonuniform coating on the optical elements, or spurious reflections within the interferometer loop.

A plot with unbalanced intensities ($\theta=-70°$) shows the tunability of the intensity for different analysis angles. As predicted in Fig. 3, a very symmetric profile occurs for $\theta=-63.5°$, allowing us to match the local maxima and minima intensities from theoretical estimates and experiment over all values of w, as discussed in greater detail below. Finally, when the analyzer is set to $-45°$, the fringes appear only in what should be the shadow region, as expected from Fig. 3.

To determine the phase *quantitatively*, we took extra photographs of the beam profile for $\theta=-45°$. Raw data are shown in Fig. 6 for the following configurations, both with and without the straight edge (in the V path): H path (V path blocked with cardboard), V path (H path blocked), and combined intensities. The green (online) solid curves are a Gaussian profile fit to the raw data. From plots 1 and 2 we can see the nearly equal intensities in the counterpropagating beams but also the noise on the beam profiles. Nevertheless, plot 3 displays nearly perfect destructive interference obtained when both paths are open and no knife edge is in place. For a beam initially polarized at

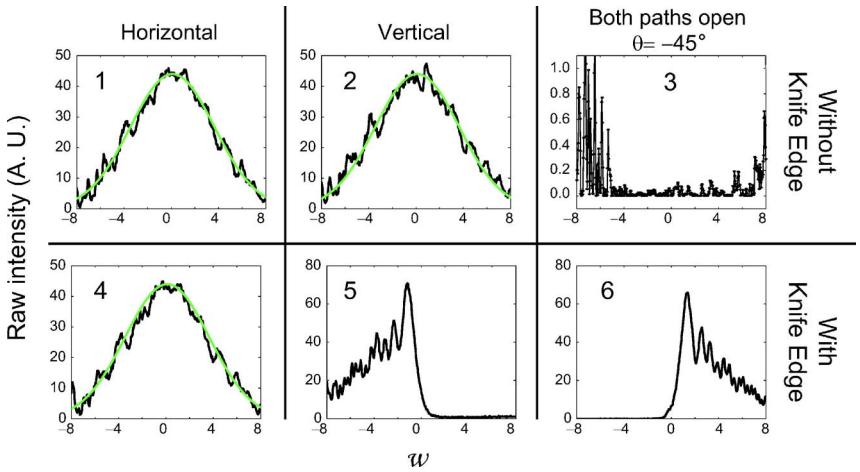

Fig. 6. (Color online) Intensity profiles used to determine the phase ϕ [from Eq. (7)] and the amount of noise in the experimental data. Note the reduced scale for panel 3 (destructive interference). Black curves correspond to experimental data, and the gray (green online) curves in panels 1, 2, and 4 are the best-fit Gaussian envelope function.

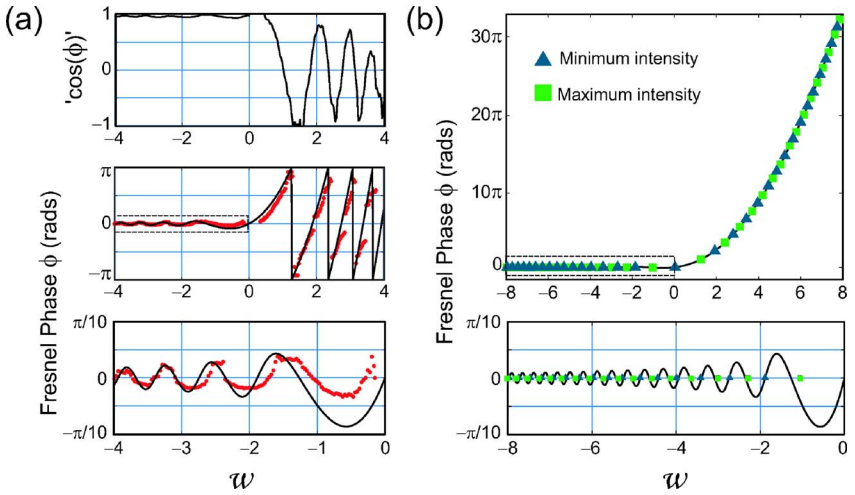

Fig. 7. (Color online) (a) "cos ϕ" function and the Fresnel phase (dots) as obtained from raw data with the polarization analyzer at −45°. Solid curve in the phase plot corresponds to the Fresnel phase as predicted using Cornu's spiral. (b) From the symmetric data, taken with the analyzer at −63.5°, we were able to match local minima (triangles) and maxima (squares) from experiment to the plane-wave theory. The lowest panels depict a zoom-in of the dashed rectangle regions, for which $w \leq 0$ (*nonshadow* region).

45° and analyzed at $\theta = -45°$, we expect the intensity to be zero and find this to be nearly the case over most w ($|w| < 4$) in the analyzed range; even for $|w| \geq 4$ the discrepancies are at most 10%. The location of the knife edge (right side of the beam) is apparent from Fig. 6, plot 5, showing the vertically polarized beam. The inversion of the intensity profile as described above occurs when both paths are open (plot 6).

By analyzing the data of these plots using Eq. (7), we can obtain the (approximate) $\cos\phi$ term, shown in Fig. 7(a). Due to noise, for some values this function has an absolute value greater than one, and therefore it is not a true cosine. From Fig. 6 plot 3 we see the highest level of noise occurs for $|w| > 4$; therefore, we expect the most precise phase determination for $|w| < 4$. The lowest panel in Fig. 7(a) displays the phase over the *nonshadow* region, where this phase is nominally quite small (note the vertical scale). Our data show reasonably good agreement for the locations of the maxima and minima. However, the experimental phase curve (dots) is slightly offset from the theoretical prediction. Moreover, some of the valleys appear wider than the peaks. We attribute this to the fact that we are necessarily employing three different data sets (Fig. 6, panels 4–6) to reconstruct the cosine expression by means of Eq. (7), so small errors on each of those intensity profiles unavoidably propagate during the phase reconstruction. (Specifically, our experiment is not optimized to detect small deviations of ϕ from zero because $\cos\phi$ is so insensitive in this region; a modified setup, with an extra $\pi/2$ phase shift applied, could be used to remove this insensitivity.)

Figure 7(b) displays the positions of the maximum (squares) and minimum (triangles) intensities from our data when the analyzer setting is −63.5°, along with the phase predicted from Cornu's spiral. This plot of the raw phase clearly shows a *quadratic* increase of the phase as $w \to \infty$, i.e., in the shadow region. We consider the over- all agreement between the experimental profile and the the-

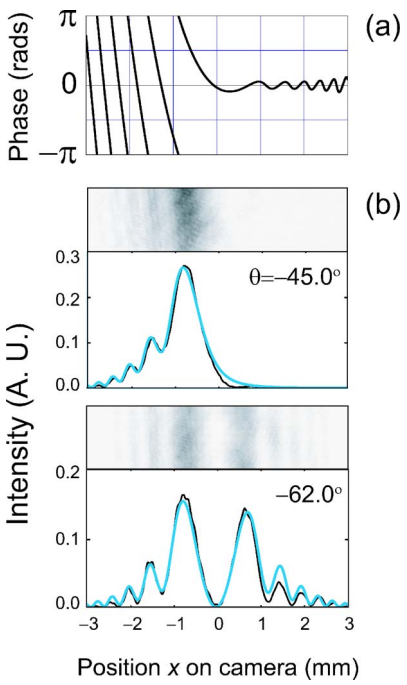

Fig. 8. (Color online) (a) Theoretical phase from straight-edge diffraction for a focused beam, (b) Intensity profiles for two analyzer settings. Experimental curves are in black, theoretical curves in gray (blue online).

oretical prediction for this analysis angle, in particular highlighted by the exceptional matching between local minima, and maxima, to be a further confirmation of the scalar theory for the phase in Fresnel diffraction.

B. Intensity Profiles for Focused Beams

Because the theoretical predictions depend strongly on the focusing of the beam and since such focusing is a common practical situation,[1] we explored this regime by inserting a lens before the interferometer. The focal length was 25 cm, leading to a focused spot size of $W_0 \sim 30$ μm after the plane of the knife edge ($z_1 = -6.7$ cm). The corresponding Rayleigh range is $Z_0 = 4.5$ mm. We make use of Eqs. (3) and (7) to obtain the theoretical intensity patterns incorporating the theory for focused Gaussian beams, developed in Appendix A.

The theoretical phase for focused beams as well as theoretical and experimental intensity profiles for two analyzer settings are shown in Fig. 8. Because we are now applying the general Gaussian beam formulas, w is a complex number; therefore, we plotted the profiles as a function of the x coordinate in the CCD camera. Here no additional *ad hoc* envelope multiplies the theoretical intensity—the focused-beam theory gives a parameter-free envelope and phase profile. Farther away from the beam's center the plane-wave approximation no longer holds, resulting in larger phase oscillations, in contrast with the decreasing phase oscillations in the plane-wave case [cf. Fig. 2(b) for $w \sim -4$]. Notice that focusing not only produces a waist, but it also *inverts* the image, cf., Figs. 8 and 5, the focused and nonfocused cases with $\theta = -45°$, whose images are approximately inverted. The theory and experiment are again in quite good agreement.

6. CONCLUSIONS

In this paper, we have presented a technique for phase determination in the near-field regime for Gaussian beams. The polarization labeling of the beams in a modified Sagnac interferometer and subsequent erasure by an analyzing polarizer allowed us to very precisely control the relative intensities of the interfering beams, thereby locally improving the interference visibility dramatically, particularly in the so-called shadow region. The experimental technique is useful for phase determination, as the enhanced visibility allows one to distinguish genuine intensity variations due to the Fresnel diffraction from output noise. Moreover, the technique is easily implemented, compatible with focused beams, and very stable, requiring no active electromechanical elements.

We obtained very good agreement with theoretical predictions for an unfocused Gaussian beam with a somewhat large Rayleigh range. Despite the inherent noise on the intensities of the interfering beams, the phase information could be retrieved fairly accurately for w in the $(-4, 4)$ range. The locations of the maximum and minimum intensities, and therefore the phase, were also in agreement when focused beams were employed. Thus the technique and accompanying general theory could be of use in realistic conditions for optical information-processing applications. Finally, although our system dealt only with 1-D diffraction, the methods presented here could obviously be extended to cover obstacles with arbitrary shape.

APPENDIX A

Here we provide the necessary steps to obtain Eq. (3) from Eq. (2). By explicitly placing $\mathcal{U}_0$ from Eq. (1) into Eq. (2), we obtain

$$U_d(\boldsymbol{\rho},z) = -\frac{kAZ_0\, e^{ikz}}{2\pi(z-z_1)q(z_1)}\int_{-\infty}^{+\infty} dy' \int_{x_1}^{+\infty} dx' \times \exp\left[\frac{ik}{2q(z_1)}\rho'^2\right]\exp\left[\frac{ik(\boldsymbol{\rho}-\boldsymbol{\rho}')^2}{2(z-z_1)}\right]. \tag{A1}$$

We now rearrange the exponent inside the integrals in Eq. (A1) to facilitate its evaluation. It takes the form

$$\frac{ik}{2(z-z_1)}\left[\alpha\left(\boldsymbol{\rho}' - \frac{\boldsymbol{\rho}}{\alpha}\right)^2 + \left(1-\frac{1}{\alpha}\right)\rho^2\right], \tag{A2}$$

where $\alpha = q(z)/q(z_1)$. Then Eq. (A1) becomes

$$U_d(\boldsymbol{\rho},z) = \frac{-kAZ_0\, e^{ikz}}{2\pi(z-z_1)q(z_1)}\exp\left[\frac{ik}{2q(z)}\rho^2\right] \times \int_{-\infty}^{+\infty} dy' \exp\left[\frac{ik\alpha(y'-y/\alpha)^2}{2(z-z_1)}\right] \times \int_{x_1}^{+\infty} dx' \exp\left[\frac{ik\alpha(x'-x/\alpha)^2}{2(z-z_1)}\right]. \tag{A3}$$

The integral over y' can be performed to give $[2\pi i(z-z_1)/k\alpha]^{1/2}$, while the integral over x' can be written as follows:

$$\int_{x_1}^{+\infty} \mathrm{d}x' \exp\left[\frac{ik\alpha\left(x'-\frac{x}{\alpha}\right)^2}{2(z-z_1)}\right] = \int_0^{+\infty} \mathrm{d}x'' \exp\left[\frac{ik\alpha x''^2}{2(z-z_1)}\right] - \int_0^{x_1-(x/\alpha)} \mathrm{d}x'' \exp\left[\frac{ik\alpha x''^2}{2(z-z_1)}\right] = \sqrt{\frac{2\pi(z-z_1)}{-ik\alpha}}\left\{\frac{1}{2} - \sqrt{\frac{-ik\alpha}{2\pi(z-z_1)}}\int_0^{x_1-(x/\alpha)} \mathrm{d}x'' \times \exp\left[\frac{ik\alpha x''^2}{2(z-z_1)}\right]\right\}, \tag{A4}$$

where $x''=x'-x/\alpha$, so that Eq. (A3) takes the form

$$U_d(\boldsymbol{\rho},z) = -\frac{iAZ_0\, e^{ikz}}{q(z)} \exp\left[\frac{ik}{2q(z)}\rho^2\right]\left\{\frac{1}{2} - \sqrt{\frac{-ik\alpha}{2\pi(z-z_1)}}\int_0^{x_1-(x/\alpha)} \mathrm{d}x' \exp\left[\frac{ik\alpha x'^2}{2(z-z_1)}\right]\right\}. \tag{A5}$$

The term

$$\mathcal{U}_0(\boldsymbol{\rho},z) = -\frac{iAZ_0\, e^{ikz}}{q(z)} \exp\left[\frac{ik}{2q(x)}\rho^2\right]$$

is just the amplitude of a Gaussian beam, Eq. (1). The final step consists of an extra change of variables $\pi t^2 \equiv [k\alpha/(z-z_1)]x'^2$ to obtain

$$U_d(\boldsymbol{\rho},z) = \frac{\mathcal{U}_0(\boldsymbol{\rho},z)}{2}\left\{1 + (i-1)\int_0^w \mathrm{d}t \exp\left[\frac{i\pi t^2}{2}\right]\right\} = \frac{\mathcal{U}_0(\boldsymbol{\rho},z)}{2}\{1 + (i-1)[C(w) + iS(w)]\}, \tag{A6}$$

with $C(w)$ and $S(w)$ ad defined in Eqs. (4) and w as defined in Eq. (5).

ACKNOWLEDGMENTS

We acknowledge the facilities at Los Alamos National Laboratory for the completion of this work. Salvador Barraza-Lopez also thanks Fundación Hertel and Olga Leticia Hernández at the Instituto Politécnico Nacional (Mexico).

Authors may be reached by e-mail at the following addresses: S. Barraza-Lopez, salva@vt.edu; D. F. V. James, dfvj@physics.utoronto.ca; P. G. Kwiat, kwiat@uiuc.edu.

REFERENCES

1. M. Mansuripur, *The Physical Principles of Magneto-Optical Recording*, 1st ed. (Cambridge U. Press. 1998).
2. W. Treimer, M. Strobl, and A. Hilger, "Observation of edge diffraction with a double crystal diffractometer," Cryst. Res. Technol. **37**, 727–733 (2002).
3. Z. Ping, G. Wei-Jian, and Y. Jian-Ping, "Diffracted field distribution from a knife-edge truncated semi-Gaussian beam as an atomic (molecular) mirror," Chin. Phys. **15**, 116–125 (2006).
4. R. W. Boyd and D. T. Moore, "Interferometric measurement of the optical phase distribution for Fresnel diffraction by a straightedge," Appl. Opt. **18**, 2013–2016 (1979).
5. T. J. Herzog, P. G. Kwiat, H. Weinfurter, and A. Zeiliriger, "Complementarity and the quantum eraser," Phys. Rev. Lett. **75**, 3034–3037 (1995).
6. J. E. Pearson, T. C. McGill, S. Kurtin, and A. Yariv, "Diffraction of Gaussian laser beams by a semi-infinite plane," J. Opt. Soc. Am. **59**, 1440–1445 (1969).
7. M. Born and E. Wolf, *Principles of Optics*, 7th ed. (Cambridge U. Press, 1999).
8. R. Sambasivan, "Diffraction of focused laser beams," Opt. Acta **21**, 323–328 (1974).
9. J. A. Murphy and A. Egan, "Examples of Fresnel diffraction using Gaussian modes," Eur. J. Phys. **14**, 121–127 (1993).
10. L. E. R. Petersson and G. S. Smith, "Three-dimensional electromagnetic diffraction of a Gaussian beam by a perfectly conducting plane," J. Opt. Soc. Am. A **19**, 2265–2280 (2002).
11. P. W. Milonni and J. H. Eberly, *Lasers*, 1st ed. (Wiley, 1988), Chap. 14.5.
12. J. W. Goodman, *Introduction to Fourier Optics*, 2nd ed. (McGraw-Hill, 1996), Chap. 4.2.
13. D. A. Jackson, A. D. Kersey, and A. C. Lewin, "Fibre gyroscope with passive quadrature detection," Electron. Lett. **20**, 399–401 (1984).
14. M. A. Novikov, "Polarization ring interferometer–ellipsometer," Opt. Spektrosk. **61**, 424–427 (1986).
15. K.-X. Sun, M. M. Fejer. E. Gustafson, and R. L. Byer, "Sagnac interferometer for gravitational-wave detection," Phys. Rev. Lett. **76**, 3053–3056 (1996).
16. P. T. Beyersdorf, M. M. Fejer, and R. L. Byer, "Polarization Sagnac interferometer with a common-path local oscillator for heterodyne detection," J. Opt. Soc. Am. B **16**, 1354–1358 (1999).
17. T. Shirai, T. H. Barnies, and T. G. Haskel, "Surface-profile measurement by means of a polarization Sagnac interferometer with parallel optical feedback," Opt. Lett. **24**, 297–299 (1999).
18. J. Xia, P. T. Beyersdorf, M. M. Fejer, and A. Kapitulnik, "Modified Sagriac interferometer for high-sensitivity rnagneto-optic measurements at cryogenic temperatures," Appl. Phys. Lett. **89**, 062508 (2006).
19. T. Kim, M. Fiorentino, and F. N. C. Wong, "Phase-stable source of polarization-entangled photons using a polarization Sagnac interferometer," Phys. Rev. A **73**, 012316 (2006).
20. P. G. Kwiat, J. R. Mitchell, P. D. D. Schwindt, and A. G. White, "Grover's search algorithm: an optical approach," J. Mod. Opt. **47**, 257–266 (2000).